

## MIT Open Access Articles

*Evidence for widespread hydrated minerals on asteroid (101955) Bennu*

The MIT Faculty has made this article openly available. **Please share** how this access benefits you. Your story matters.

**Citation:** Hamilton, V.E., et al., "Evidence for widespread hydrated minerals on asteroid (101955) Bennu." *Nature astronomy* 3, 4 (2019): p. 332-340 doi 10.1038/s41550-019-0722-2 ©2019 Author(s)

**As Published:** 10.1038/s41550-019-0722-2

**Publisher:** Springer Science and Business Media LLC

**Persistent URL:** <https://hdl.handle.net/1721.1/124501>

**Version:** Author's final manuscript: final author's manuscript post peer review, without publisher's formatting or copy editing

**Terms of use:** Creative Commons Attribution-Noncommercial-Share Alike





Published in final edited form as:

*Nat Astron.* 2019 ; 3(4): 332–340. doi:10.1038/s41550-019-0722-2.

## Evidence for widespread hydrated minerals on asteroid (101955) Benu

V. E. Hamilton<sup>\*1</sup>, A. A. Simon<sup>2</sup>, P. R. Christensen<sup>3</sup>, D. C. Reuter<sup>2</sup>, B. E. Clark<sup>4</sup>, M. A. Barucci<sup>5</sup>, N. E. Bowles<sup>6</sup>, W. V. Boynton<sup>7</sup>, J. R. Brucato<sup>8</sup>, E. A. Cloutis<sup>9</sup>, H. C. Connolly Jr.<sup>10</sup>, K. L. Donaldson Hanna<sup>6</sup>, J. P. Emery<sup>11</sup>, H. L. Enos<sup>7</sup>, S. Fornasier<sup>5</sup>, C. W. Haberle<sup>3</sup>, R. D. Hanna<sup>12</sup>, E. S. Howell<sup>7</sup>, H. H. Kaplan<sup>1</sup>, L. P. Keller<sup>13</sup>, C. Lantz<sup>14</sup>, J.-Y. Li<sup>15</sup>, L. F. Lim<sup>2</sup>, T. J. McCoy<sup>16</sup>, F. Merlin<sup>5</sup>, M. C. Nolan<sup>7</sup>, A. Praet<sup>5</sup>, B. Rozitis<sup>17</sup>, S. A. Sandford<sup>18</sup>, D. L. Schrader<sup>3</sup>, C. A. Thomas<sup>19</sup>, X.-D. Zou<sup>15</sup>, D. S. Lauretta<sup>7</sup>, OSIRIS-REx Team

<sup>1</sup>Department of Space Studies, Southwest Research Institute, Boulder, CO, USA

<sup>2</sup>NASA Goddard Space Flight Center, Greenbelt, MD, USA

<sup>3</sup>School of Earth and Space Exploration, Arizona State University, Tempe, AZ, USA

<sup>4</sup>Department of Physics and Astronomy, Ithaca College, Ithaca, NY, USA

<sup>5</sup>LESIA, Observatoire de Paris, France

<sup>6</sup>Department of Atmospheric, Oceanic and Planetary Physics, University of Oxford, Oxford, UK

<sup>7</sup>Lunar and Planetary Laboratory, University of Arizona, Tucson, AZ, USA

<sup>8</sup>INAF-Astrophysical Observatory of Arcetri, Firenze, Italy

<sup>9</sup>Department of Geography, University of Winnipeg, Winnipeg, Canada

<sup>10</sup>Department of Geology, Rowan University, Glassboro, NJ, USA

<sup>11</sup>Department of Earth and Planetary Science, University of Tennessee, Knoxville, TN, USA

<sup>12</sup>Jackson School of Geosciences, University of Texas, Austin, TX, USA

<sup>13</sup>ARES, NASA Johnson Space Center, Houston, TX USA

---

\*Corresponding author: hamilton@boulder.swri.edu.

### Author Contributions

V.E.H. is the spectral analysis working group lead, the OTES Deputy Instrument Scientist, and wrote this manuscript. A.A.S. is the spectral analysis working group deputy, the OVIRS Deputy Instrument Scientist, and led the calibration of the OVIRS data and production of the disk-integrated average spectrum. P.R.C. is the OTES Instrument Scientist and led the calibration of OTES data. D.C.R. is the OVIRS Instrument Scientist. B.E.C. is the OSIRIS-REx Mission Asteroid Scientist. M.A.B., H.H.K., R.D.H., and A. P. contributed to the analysis of the OVIRS 2.7  $\mu\text{m}$  band. N.E.B. hosts the laboratory that made the simulated asteroid environment spectral measurements. W.V.B. is the Mission Instrument Scientist and contributed to ensuring the mission plan enables the instruments to meet their observation requirements. J.R.B., E.A.C., S. F., C. L., J.-Y.L., F.M., S.A.S., C.A.T., and Z.-D. Z. contributed to the development of science pipeline software. H.C.C., Jr. is the Mission Sample Scientist and helped guide the selection and acquisition of the meteorite samples used in this work. K.L.D.H. measured the samples shown in Figure 4b. J.P.E. and B. R. contributed to the subtraction of thermal emission from OVIRS spectra. H.L.E. is the Deputy Principal Investigator for the OSIRIS-REx mission. C.W.H. contributed to the data processing and analysis of OTES spectra. E.S.H. contributed to the development of science pipeline software and provided manual processing of some of the data shown in this manuscript. L.P.K. and T.J.M. helped guide the selection and acquisition of the meteorite samples used in this work. L.F.L. contributed to extensive discussions about the laboratory measurements. M.C.N. is the Science Team Chief and contributed the resampled solar spectrum used in the calibration of OVIRS data. D.L.S. contributed to the preparation and characterization of meteorite samples used in this work. D.S.L. is the OSIRIS-REx Principal Investigator and the entire OSIRIS-REx Team made the Benu encounter possible.

<sup>14</sup>Institut d'Astrophysique Spatiale, CNRS/Université Paris Sud, Orsay, France

<sup>15</sup>Planetary Science Institute, Tucson, AZ, USA

<sup>16</sup>Smithsonian Institution, National Museum of Natural History, Washington, D.C., USA

<sup>17</sup>Planetary and Space Sciences, The Open University, Milton Keynes, UK

<sup>18</sup>NASA Ames Research Center, Moffett Field, CA, USA

<sup>19</sup>Department of Physics and Astronomy, Northern Arizona University, Flagstaff, AZ, USA

## Abstract

Early spectral data from the Origins, Spectral Interpretation, Resource Identification, and Security–Regolith Explorer (OSIRIS-REx) mission reveal evidence for abundant hydrated minerals on the surface of near-Earth asteroid (101955) Bennu in the form of a near-infrared absorption near 2.7  $\mu\text{m}$  and thermal infrared spectral features that are most similar to those of aqueously altered CM carbonaceous chondrites. We observe these spectral features across the surface of Bennu, and there is no evidence of substantial rotational variability at the spatial scales of tens to hundreds of meters observed to date. In the visible and near-infrared (0.4 to 2.4  $\mu\text{m}$ ) Bennu's spectrum appears featureless and with a blue (negative) slope, confirming previous ground-based observations. Bennu may represent a class of objects that could have brought volatiles and organic chemistry to Earth.

---

The OSIRIS-REx mission began its Approach phase to asteroid (101955) Bennu in August 2018. Before and just after arrival at Bennu on 3 December, the OSIRIS-REx Visible and InfraRed Spectrometer (OVIRS) and Thermal Emission Spectrometer (OTES) collected hyperspectral data of this B-type asteroid, which is thought to be related to the carbonaceous chondrite meteorites<sup>1</sup>. The OVIRS instrument<sup>2</sup> is a hyperspectral, point spectrometer that measures the reflected and emitted energy of Bennu across the spectral region from 0.4 to 4.3  $\mu\text{m}$  (25,000 to 2,300  $\text{cm}^{-1}$ ) with a circular, 4-mrad field of view (FOV). The OTES instrument<sup>3</sup>, the first thermal infrared spectrometer to visit an asteroid, is a hyperspectral, point spectrometer that measures the emitted radiance of Bennu across the spectral region from  $\sim 1750$  to 100  $\text{cm}^{-1}$  ( $\sim 5.71$  to 100  $\mu\text{m}$ ) with a circular, 8-mrad FOV. The primary role of visible-to-infrared spectroscopy on the OSIRIS-REx mission is to characterize the mineralogy and chemistry of Bennu and aid in sample site selection<sup>4</sup>. The OTES radiance data also are used in conjunction with thermophysical models to determine properties of the surface, such as particle size and roughness, and to study the Yarkovsky effect<sup>5</sup>. The mineralogy and chemistry of the surface of Bennu provide information about the geological processes that have affected the asteroid, the potential for resource extraction, and the accuracy of telescopic spectral observations (with the final ground-truth coming from measurements of the returned sample).

On five days between 2 and 9 November 2018, both spectrometers obtained whole-disk (sub-FOV) spectra of Bennu for 4.5 hours, which is just over one full rotation period ( $\sim 4.3$  hours). In December 2018, both instruments collected spatially resolved spectra of Bennu as “ride-along” observations during imaging activities optimized for the PolyCam and MapCam imagers<sup>6</sup>.

## Visible and near-infrared spectral characteristics

The ground-based, composite (0.4 to 2.4  $\mu\text{m}$ ) reflectance spectrum of Bennu shows a spectrally “blue” (negative) continuum slope across the visible and near infrared, characteristic of B-type asteroids<sup>1</sup>. *Clark et al.*<sup>1</sup> did not find strong spectral absorptions in the Bennu telescopic data, and they identified CI and CM carbonaceous chondrites as the most likely spectral matches, with a preference for a CM1-like composition. (Please note that throughout the paper we following the standard convention of petrologic types for chondrites, such as CI1 and CM2, first introduced by Van Schmus and Wood<sup>7</sup>.) Thus, Bennu was predicted to have hydrated minerals, but no spectral features attributable to hydration were observed. The average OVIRS disk-integrated spectrum of Bennu compares very well with the telescopic data at these wavelengths, also having a negative slope and no clear absorption features (Figure 1). There is no variation in the spectra (above the noise) with rotational phase. Analysis of spatially resolved data is ongoing and will be used to confirm or refute ground-based observations of spectral slope changes<sup>8</sup>.

A blue-sloped continuum could be explained in one or more ways; such a continuum has been observed in some CI and CM carbonaceous chondrites and, in CI meteorites, is attributed to the presence of fine-particulate magnetite and/or insoluble organic material; it is also commonly associated with larger-particle-size samples and possibly space weathering<sup>9–11</sup>. *Lauretta et al.*,<sup>12</sup> identify a candidate magnetite feature at 0.55  $\mu\text{m}$ <sup>13</sup> in the darkest materials imaged by the MapCam instrument; however, as of yet, no such feature has been observed in OVIRS spectra that would confirm this detection or its assignment to magnetite. Such a feature may become evident in the higher-spatial-resolution OVIRS data that will be collected later in the mission. Experimental space weathering of carbonaceous materials can result in reddening or bluing of the spectral slope<sup>11,14,15</sup>; at present, we do not have sufficient information from OVIRS spectra to draw any conclusions about the nature or degree of space weathering on Bennu as it relates to Bennu’s spectral slope or the presence of magnetite.

At longer wavelengths ( $>2.4 \mu\text{m}$ ), both disk-integrated and spatially resolved OVIRS spectra display a  $\sim 2.7\text{-}\mu\text{m}$  absorption feature. The 2.7- $\mu\text{m}$  feature is apparent in all OVIRS spectra collected thus far and is similar to the feature observed in aqueously altered CM1 and CM2 carbonaceous chondrites<sup>16–19</sup>. In analog meteorites measured under appropriate conditions (Figure 2), this absorption is due primarily to structural  $-\text{OH}$  ions in hydrous clay minerals (typically poorly-ordered to crystalline phyllosilicates of the kaolinite-serpentine group), which are common in CI and CM carbonaceous chondrites<sup>19–21</sup>. Among carbonaceous chondrites, hydrated minerals also are a component of CR chondrites<sup>22</sup>. Adsorbed  $\text{H}_2\text{O}$  in CI/CM meteorite samples (commonly terrestrial in origin) exhibits a broad feature centered closer to 3.1  $\mu\text{m}$ <sup>19</sup>. Any potential  $\text{H}_2\text{O}$  feature in the OVIRS spectrum is weak and will be examined in greater detail using higher spatial resolution data.

The exact position of the  $\sim 2.7\text{-}\mu\text{m}$  band minimum in phyllosilicates shifts with mineral structure and composition<sup>19,23</sup> and there is experimental evidence that its position may be altered by space weathering<sup>24</sup>. The band center in the OVIRS data is at 2.74  $\mu\text{m}$  ( $\pm 0.01$ ). *Takir et al.*<sup>19</sup> showed that CI and CM chondrites display three distinct types of spectra based

on the position of this feature. In “Group 1” spectra, this feature ranges in position from 2.77 to 2.80  $\mu\text{m}$  and is associated with petrologic subtypes between CM2.3 and 2.6 (where decimal values indicate relative alteration within type 2, with smaller values representing greater alteration). The band center for “Group 2” meteorites ranges from 2.76 to 2.78  $\mu\text{m}$  and includes petrologic subtypes CM2.1 to 2.2, which are the most aqueously altered petrologic type 2 meteorites. Finally, “Group 3” meteorites are also CM2.1 to 2.2 but have a band center at 2.72  $\mu\text{m}$ . Ivuna, the only CI1 in the study, has a band center at 2.71  $\mu\text{m}$ . The OVIRS band center lies between Groups 2 and 3 and is consistent with meteorites having petrologic types of CM2.1 – 2.2. Meteorites with these petrologic types are among the most aqueously altered samples studied. Space weathering effects on asteroids in this spectral region do not always match predictions<sup>25</sup> but if solar wind irradiation is affecting this band in a manner consistent with experimental data on Murchison (CM2.5), the predicted effect would be to shift the band center to slightly longer wavelengths (a maximum of 0.03  $\mu\text{m}$  for Murchison) and introduce a concave shape<sup>24</sup>. As seen in Figure 2, spectra of CI and CM1 and low petrologic type CM2 meteorites can display concave shapes in the absence of irradiation. The concavity of the Bennu spectrum is visibly less than that observed in the analogue meteorites, therefore, we cannot uniquely ascertain whether or not the shape of the Bennu spectrum in this region is indicative of space weathering.

Prior studies identify four classes of so-called “3- $\mu\text{m}$  band shapes among C-complex Main belt asteroids, which includes the region of the 2.7- $\mu\text{m}$  feature. These classes are named for their type examples: the asteroids Ceres, Pallas, and Themis and the Jovian moon Europa<sup>26–29</sup>. These classes correspond to different dominant surface materials. Bennu’s spectrum, with its smooth rise from 2.85 to  $\sim$ 3.3  $\mu\text{m}$  and blue spectral slope, falls into the Pallas-like class, consistent with what is presumed to be a phyllosilicate-dominated composition.

Spectra of Cb-type<sup>30</sup> asteroid (162173) Ryugu measured by the near-infrared spectrometer on the JAXA-led Hayabusa2 mission exhibit a weak, narrow 2.72- $\mu\text{m}$  hydroxyl band that does not vary spatially and is interpreted as indicating the presence of Mg-rich phyllosilicates<sup>31</sup>. The best meteorite analogues for the observed feature are thermally-metamorphosed CI chondrites and shocked CM chondrites, suggesting that Ryugu has experienced more heating than Bennu, although other interpretations are possible<sup>31</sup>. Regardless of the interpretation, it is clear that Ryugu differs from unheated or slightly heated, phyllosilicate-rich carbonaceous chondrites and from Bennu.

There is not yet unambiguous evidence of organic features in the whole-disk or spatially resolved OVIRS spectra of Bennu above the level of the noise in the data shown. The whole-disk observations filled only  $\sim$ 40% of the FOV, and the spatially resolved data were acquired at moderate phase angles ( $\sim$ 40–50°) on relatively hot ( $\sim$ 340 K) surfaces, which increases the contribution from thermal emission at the wavelengths where organic bands would be expected. Planned higher-spatial-resolution data on colder surfaces may yet reveal such signatures.

## Thermal infrared spectral characteristics

Whole-disk emissivity spectra of Bennu acquired in 2007 by the Infrared Spectrograph on the Spitzer Space Telescope have no discernible spectral features above the noise level of the data<sup>32</sup> although a comparison is shown by<sup>33</sup>. Comparable disk-integrated OTES observations require additional calibration because Bennu does not fill the OTES FOV. However, spatially resolved (80 m/spot) OTES observations reveal thermal infrared (TIR) spectra having a spectral contrast of ~2% that do not vary in shape with rotational phase above the level of the noise (Figure 3).

The average TIR spectrum of Bennu exhibits a Christiansen feature (a peak on the high wavenumber/short wavelength side of the first major, usually silicate, absorption) position that is most similar to that of the CM1/2 and CM2 petrologic types. The spectrum also exhibits an absorption at the lowest wavenumbers (longest wavelengths) that is very similar to that observed in CI and CM carbonaceous chondrites (Figure 4). Meteorites in the CI and CM groups are volumetrically dominated (>55 vol.%<sup>34,35</sup>) by hydrated silicate minerals of the phyllosilicate group and are widely accepted to have been aqueously altered during their history within a parent body<sup>36–38</sup>. Therefore, we can infer that Bennu's surface is volumetrically dominated by phyllosilicates and represents aqueous alteration of the parent body.

It is notable that we have not yet observed a distinct Mg-OH feature near  $625\text{ cm}^{-1}$  ( $16\text{ }\mu\text{m}$ ), as this feature is common to many meteorites of the CI and CM groups. The absence of this feature may be indicative of a non-Mg endmember (Fe-bearing) phyllosilicate composition, modest heating, disorder, and/or a particle size effect. Although there is no “smoking gun” match to Bennu among the aqueously altered meteorites, spectra of Bennu are distinctly dissimilar to carbonaceous meteorite groups that have either not undergone hydrothermal aqueous alteration or have experienced alteration but are now “dry” (e.g., CO, CB, CV, CK<sup>39</sup>) (Figure 4 and Methods). Bennu's spectral signature also is dissimilar to meteorites of the CR group, which may be aqueously altered but typically contain lesser amounts of phyllosilicates with abundant olivine and pyroxene<sup>34</sup> and have features that would be evident in the Bennu spectrum (Figure 4)<sup>39–41</sup>.

OTES spectra of Bennu also exhibit two features at  $555$  and  $340\text{ cm}^{-1}$  that are likely attributable, at least in part, to magnetite (Figure 5) and may support the proposed detection of a magnetite feature at  $\sim 0.55\text{ }\mu\text{m}$  in the darkest regions of the asteroid<sup>12</sup>. Magnetite is believed to be a product of aqueous alteration and is present at abundances up to  $\sim 10\%$  in CI chondrites. Magnetite abundance varies widely in CM chondrites, from  $\sim 0.3$  –  $8.4\%$  depending on petrologic subtype<sup>34,35</sup>. The abundance of magnetite on Bennu has not yet been tightly constrained, but it is present at abundances of at least a few percent and its detection is consistent with our other observations that support an affinity with these meteorite groups.

The spectral slope of Bennu from  $1500$  to  $1110\text{ cm}^{-1}$  ( $\sim 6.6$  to  $9\text{ }\mu\text{m}$ ) is relatively shallow and featureless—it does not clearly exhibit the spectral shapes and emissivity reductions in this region that are common to fine-particulate sample spectra and result from volume

scattering (Figure 4b). The region of silicate stretching bands ( $\sim 1100$  to  $700\text{ cm}^{-1}$ ;  $\sim 9$  to  $14.3\text{ }\mu\text{m}$ ) exhibits a broad, bowl-like shape that is not well reproduced by spectra equivalent to solid and coarse-particulate (e.g.,  $>125\text{ }\mu\text{m}$ ) meteorites or fine-particulate ( $<125\text{ }\mu\text{m}$ ) meteorites measured in vacuum with an induced thermal gradient (Figure 4). Although there are similarities in the shape and breadth of the fine-particulate Orgueil (CI) chondrite spectrum and Bennu in this region, there are distinct differences between these spectra at higher wavenumbers, so this feature shape might alternatively indicate an amorphous/disordered component rather than production of transparency features resulting from volume scattering.

Despite the lack of strong evidence for abundant, volume-scattering (fine) particulates at the  $\sim 80\text{-m}$  spatial scale of these observations, it is possible that these spectra represent a mixture of a small amount of fine ( $<125\text{ }\mu\text{m}$ ) and greater amount of coarse ( $>125\text{ }\mu\text{m}$ ) particulate materials, as well as the boulders that are present across the surface<sup>5,42</sup>. The lack of variation in the spectra indicates that at these spatial scales, the distribution of particle sizes on the surface does not vary substantially. The thermal inertia of Bennu is  $350 \pm 20\text{ J m}^{-2}\text{ K}^{-1}\text{ s}^{-1/2}$ , does not vary with rotational phase, and indicates a mean particle size on the order of  $0.5$  to  $5\text{ cm}^5$ . However, thermal inertia is not uniquely interpretable in terms of particle size, and the presence of numerous boulders for this relatively low value of thermal inertia could be interpreted as indicating that there also may be smaller particles present than the mean particle size estimate would suggest. On the other hand, it may be that the assumption about the thermal inertia of boulders on Bennu is inaccurate and that their thermal inertia is lower than what is assumed for typical planetary materials<sup>5</sup>. The lack of rotational variability in thermal inertia is consistent with the lack of variability in the apparent particle size distribution from spectroscopy, despite their differing depth sensitivities.

OSIRIS-REx spectroscopic observations from visible through thermal infrared wavelengths are highly complementary and show that the pristine sample that will be returned from Bennu has the potential to inform our understanding of water in the early solar system and its origins on Earth. Bennu's spectra indicate that the surface is consistent with and dominated volumetrically by some of the most aqueously altered CM chondrites. We cannot rule out the presence of a lesser component of CI material based on both the presence of magnetite and the visual variability among materials on the surface<sup>5</sup>.

The spectral datasets presented here are consistent with a surface having range of particle sizes that does not vary spatially at scales down to  $80\text{ m}$  as evidenced by the lack of variation in the spectral reflectance and emissivity. Other observed properties may help explain the apparent spatial uniformity of the spectral signatures at relatively large scales if there are compositional variations present among the mobile materials, but material movement leads to homogenization of their distribution. The lack of rotational and spatial variation in particle size distribution may reflect surficial redistribution processes rather than compositional uniformity, given the observed variations in albedo<sup>5</sup>. Redistribution processes are supported by the geopotential at Bennu's surface, which reveals that disturbed material moves towards the equator and/or escapes<sup>43</sup>. Additionally, analysis of the geological characteristics of Bennu's surface indicates that it is an old rubble pile but has experienced recent dynamical and geological processes<sup>42</sup>. With these and future, higher-spatial-

resolution spectral observations, we will be able to 1) provide vital context for analysis of the returned sample; 2) address the history and degree of aqueous alteration experienced by Bennu's parent body based on details of mineral distribution, abundance, and composition (e.g., Mg/Fe proportions in phyllosilicates and abundance of magnetite); and 3) constrain the presence or absence of organics.

## Methods

### OVIRS instrument, calibration, and data processing

The OVIRS design is derived from the New Horizons LEISA portion of the Ralph instrument<sup>44</sup> with an extended wavelength and simplified optics. The spectrometer uses five linear variable filters to collect the spectrum. Details of the various operating modes (e.g., super pixel summing) are described elsewhere<sup>2</sup>. To measure compositional spectral features with >5% absorption depth at spatial resolutions of 5 to 50 m, OVIRS meets a performance requirement of a signal-to-noise ratio (SNR) of >50 across the entire spectral range assuming an asteroid surface albedo of ~3–4% at a solar range of 1.2 AU and 300 K thermal radiation. To characterize and map variations in space weathering on surfaces with an albedo of >1%, OVIRS meets an accuracy requirement of 2.5% with a precision of 2%. OVIRS calibrations and performance assessments were performed on the ground and in-flight during the OSIRIS-REx Earth encounter in September 2017<sup>45</sup>.

The observing sequence on day of year (DOY) 306 consisted of pointing OVIRS at Bennu for 4.5 hours while scanning in a slight “up and down” pattern but keeping Bennu within the FOV at all times to obtain whole-disk measurements. The phase angle during these observations was ~5.2°. The spectrum shown in Figures 1 and 2 is the average of 17,061 radiance factor (RADF) or I/F spectra where Bennu filled approximately 40% of the FOV; the excursions in the spectra are representative of the point-to-point scatter in the data. The OVIRS calibrated radiance spectra were obtained according to methods described by<sup>2,45</sup>. In brief, OVIRS raw data are converted from counts/second to absolute radiance units using an automated calibration pipeline. First, the closest space view is identified to create an average background file. The background subtracted counts are converted to physical units using radiometric and out-of-band coefficients derived from ground testing and in-flight calibration activities. The full calibration approach is described in more detail elsewhere<sup>45</sup>. Slight adjustments were made to the previously derived radiometric and out-of-band coefficients to adjust the response in a few spectral regions based on the Bennu Approach data to ensure filter overlap regions aligned. Calibrated radiances are then resampled onto a common wavelength axis by removing outlying noise spikes more than 1.8 standard deviations from the mean and a performing a weighted average on the remaining spectral points in each wavelength bin. The common wavelength axis has a spectral sampling of 2 nm from 0.4 to 2.4  $\mu\text{m}$  and 5 nm from 2.4 to 4.3  $\mu\text{m}$ . Data are then converted to radiance factor (I/F) by dividing by the solar spectrum scaled for Bennu's distance.

The OVIRS disk-integrated data shown in this work are not photometrically corrected. The geometric albedo of Bennu ( $0.044 \pm 0.002$ ) as determined from imaging results is given by<sup>46</sup>. The geometric albedo of asteroids (extrapolated to 0° phase) is known to be higher than the values measured in laboratory settings at 30° phase, where for Bennu's phase function, this

scale factor is  $\sim 2$ . If we apply this scaling factor to meteorite albedo values presented in Figure 4 of<sup>1</sup>, CI and CM chondrite values are most comparable to the geometric albedo of the hemispherically-integrated observation of Bennu and meteorites of the CK, CO, CV, CR, and CH groups are not consistent. However, because there is evidence in higher resolution imaging of materials on Bennu's surface having considerably higher albedos<sup>5</sup>, we are not prepared to assert that any compositions are ruled out by the global geometric albedo value.

Analysis of OVIRS spectra beyond  $\sim 2 \mu\text{m}$  requires removal of the contribution to the signal from thermal emission. We have tested two methods for removing this "thermal tail", with both giving similar results; we show the spectrum obtained by the first method. The first approach to computing the thermal contribution to the total radiance uses a smooth-surface thermophysical model assuming a spherical asteroid. The thermal portion of the measured flux was estimated assuming that the spectrum of Bennu is flat from 2.2 to 4.0  $\mu\text{m}$ . The thermal model was run while varying thermal inertia and asteroid size to fit the thermal portion of the measured flux for each OVIRS spectrum. The reflected radiance was computed as a straightforward subtraction of the model thermal radiance from the total measured radiance. In this approach, all the uncertainty and any remaining calibration artifacts are assumed to reside in the reflected radiance. Because the absolute uncertainties remain unchanged but the radiance itself is decreased substantially at wavelengths with significant thermal contribution, the relative uncertainties at these longer wavelengths increase, leading to an apparent increase in noise at longer wavelengths in the subtracted spectrum. For purposes of searching for potential spectral features, we also computed total model radiance by adding the thermal model radiance to a model reflected radiance (computed by scaling the solar spectrum to OVIRS radiance at 2.2  $\mu\text{m}$ ), then divided the measured OVIRS spectra by the model total spectra (Figures 1 and 2).

In the second method, the thermal contribution to the total radiance was computed using the OSIRIS-REx thermal model described in<sup>5</sup>. The computation was performed independently for each OVIRS spectrum for the instantaneous spacecraft distance and rotation phase of Bennu, using the shape of Bennu derived from OSIRIS-REx images<sup>47</sup>. We used the v13 shape model at the lowest (12-m) resolution. The disk-integrated thermal models are not affected by the small changes in the newer version (v20) of the shape model. For some rotation phases, the model thermal radiance does not perfectly match the OVIRS measurements due to remaining imperfections in the shape model. We therefore scaled the model thermal radiance to the average measured radiance (averaged from 3.5 to 4.0  $\mu\text{m}$ ) of each spectrum before subtracting from the total radiance. For scaling purposes, the measured thermal radiance was estimated assuming that the reflectance of Bennu is flat from 2.2 to 4.0  $\mu\text{m}$ . The reflected radiance was computed as a straightforward subtraction of the model thermal radiance from the total measured radiance. In this approach, all the uncertainty and any remaining calibration artifacts are assumed to reside in the reflected radiance as described above.

Determination of the 2.7- $\mu\text{m}$  band center was calculated (after the correction for thermal emission) using two methods that give virtually the same result to within the uncertainty of the measured spectrum. The first method is to fit a sixth-order polynomial to the measured spectrum between 2.65 and 2.85  $\mu\text{m}$  and find the minimum of that fit; this is the same

method used by<sup>19</sup> although those authors did not report the wavelength range over which they did their fitting. This fit was calculated for both versions of the average thermal-radiance-removed Bennu spectrum. The derived minima vary by a single channel between the two spectra, being fit at 2.74 and 2.745  $\mu\text{m}$ . Because the thermal emission correction can influence the position of this band, and these spectra represent a whole-disk measurement with variable temperatures and phase angles, this result suggests our uncertainty is relatively small (on the order of the channel to channel uncertainty).

The second method for determining the 2.7- $\mu\text{m}$  band position fits a smoothing spline function to the spectrum between 2.69 and 2.85  $\mu\text{m}$  for the DOY 306 (2 November 2018) average spectrum; the best fit is obtained using a smoothing value of 0.999999. The first derivative is then calculated, and the inflection point is used to determine the position of the band, which is  $2.74 \pm 0.007$ . Applying the same analytical approach to all of the spectra acquired on DOY 306, we obtain the same answer, to within the uncertainty of the data. Based on the consistency of the results obtained by these two methods and their estimated uncertainties, we conservatively identify the feature as being located at  $2.74 \pm 0.01 \mu\text{m}$ .

### OTES calibration and data processing

The OTES instrument<sup>3</sup> is a Michelson interferometer with heritage from the Mars Exploration Rovers Mini-Thermal Emission Spectrometer (Mini-TES) and Mars Global Surveyor Thermal Emission Spectrometer (TES)<sup>48,49</sup>. Spectral sampling is  $8.66 \text{ cm}^{-1}$  across the entire spectrum. To confidently identify spectral features having a  $>5\%$  band depth and achieve a 1.5% total emitted radiance accuracy requirement, OTES meets a SNR of 320 at a reference temperature of 325 K and has a single-spectrum radiometric precision of  $2.2 \times 10^{-8} \text{ W cm}^{-2} \text{ sr}^{-1} / \text{cm}^{-1}$  between 1350 and  $300 \text{ cm}^{-1}$ . The absolute integrated radiance error is  $<1\%$  for scene temperatures ranging from 150 to 380 K.

Observing sequences designed to obtain whole-disk OTES spectra consisted of pointing OTES at Bennu for 4.5 hours (a little longer than one full rotation of the asteroid) without scanning. However, the standard calibration of OTES data depends on the scene and the calibration targets all filling the FOV; when the scene (Bennu) fills only a portion of the FOV, wavelength-dependent, off-axis modulation of energy through the interferometer results in an apparent low signal at short wavelengths. Correcting this effect requires a substantially more complex calibration approach, which is under consideration. As such, we show here spectra acquired on DOY 347 (13 December 2018) when the FOV was fully filled and the standard calibration approach is appropriate for the observations. The average phase angle during these observations was  $\sim 45.5^\circ$ . The DOY 347 observations cover the equator and southern (relative to the plane of the ecliptic) hemisphere and are equally representative of observations in the northern hemisphere collected during Preliminary Survey sequences on other days.

The calibration of OTES data generally consists of an automated processing pipeline that transforms OTES raw interferograms into voltage spectra and then into absolute radiance units<sup>3</sup>. More specifically, the measured voltage spectrum is the difference between the radiance of the scene, foreoptics, and the detector times the instrument response function (IRF); the radiance of the detector and the IRF are unknowns, but can be determined by

periodically observing space and an internal calibration target, at which point it becomes possible to solve for the scene radiance and account for temperature fluctuations of the instrument (detector) that result from the instrument heater cycling during the observations. After the acquisition of Earth observations in September 2017, an adjustment was made to the calibration pipeline to account for slopes in the interferograms that occur during the transition between cold space and a hot target (e.g., Earth or Bennu). This slope results from the time constant associated with the DC-correction electronics (which is longer than the 2-second integration) and, if uncorrected, results in high-frequency “ringing” in the spectra. In addition, many of the “ride-along” observation sequences in Approach and Preliminary Survey<sup>4</sup> that were designed for imaging did not include periodic views of space, instead measuring space only at the start and end of sequences that lasted on the order of 4.5 hr. As a result, an alternative calibration approach was developed to account for instrument (detector) temperature fluctuations during these sequences; this involves using a look-up table that correlates in-flight measurements of the temperature measured by a thermistor adjacent to the detector to the detector radiance.

The afternoon local time of the DOY 347 observations (~15:00 - 15:30) results in viewing surfaces having different temperatures (e.g., sunlit and shadowed) thus requiring an emissivity-temperature separation that allows for the fitting of multiple temperatures. We fit the OTEC calibrated radiances using a non-negative linear least squares algorithm<sup>50</sup> that takes as input a suite of Planck functions having temperatures between 150 and 380 K. The mixture of Planck functions that provides the best fit to the measured radiance is divided into the measured Bennu radiances to obtain emissivity, where the maximum emissivity is assumed to be 0.97 based on reflectance measurements of relevant carbonaceous chondrite meteorites<sup>39</sup>. The Bennu spectrum shown in Figures 3 and 4 is the average of 974 spectra having spatial resolutions of ~80–90 m/spot collected on DOY 347.

### Meteorite samples

The meteorites shown in Figure 2 are Ivuna (CI1), LaPaz Icefield (LAP) 02277 (CM1), Meteorite Hills (MET) 00639 (CM2), and Cold Bokkeveld (CM2)<sup>19</sup>. Cold Bokkeveld may have been very mildly and briefly heated based on Raman spectroscopy of the insoluble organic material, but the evidence is somewhat ambiguous<sup>51,52</sup> and there is no mineralogical evidence of heating that would change our interpretation of the observed 2.71- $\mu\text{m}$  feature (where mineralogy is the property to which the laboratory and remote sensing measurements shown here are sensitive). Because meteorites have interacted with the Earth’s environment, even if briefly, they are prone to mineralogical and chemical alteration, including the adsorption and absorption of terrestrial water (which can be recognized through oxygen isotope analysis). The spectra shown in Figure 2 were measured under vacuum after the samples were heated to between 400 and 475 K, which drives out adsorbed and absorbed terrestrial water. The laboratory spectra have been resampled to the OVIRS spectral sampling. See<sup>19</sup> for details of sample preparation, characterization, and measurement.

The meteorites shown in Figure 4 are Orgueil (CI1), Allan Hills (ALH) 83100 (CM1/2), Murchison (CM2), Miller Range (MIL) 090001 (CR2), Allende (CV3<sub>ox</sub>), and Vigarano (CV3<sub>red</sub>). All of these spectra were acquired as part of the development of the OSIRIS-REx

spectral library for the analysis of OTES data and have been resampled to the OTES spectral sampling. The spectral acquisition methods are described below. The text indicates that thermal infrared spectra of meteorite groups CO, CB, and CK do not resemble the OTES spectrum of Bennu; spectra of these groups are contained in the research collection of V.E.H. and are not shown here but have been shown elsewhere<sup>39</sup>.

### Laboratory spectroscopy

The meteorite spectra shown in Figure 4a were measured by V.E.H. in reflectance on uncoated thin sections using a Thermo Scientific Nicolet iN10 microscope at Southwest Research Institute in Boulder, CO. The microscope is equipped with a KBr beamsplitter and a nitrogen-cooled, extended-range mercury-cadmium-telluride (MCT) detector and measures spectra from 4,000 to 400  $\text{cm}^{-1}$ ; the optical geometry of this microscope is such that the spectra are equivalent to emission spectra according to Kirchhoffs Law<sup>53</sup>. The spectra have been scaled by differing amounts to minimize spectral contrast variations and simplify the comparison of spectral shapes. These spectra are appropriate for comparison to OTES emissivity spectra of coarse particulates and solids that do not exhibit volume scattering and are not susceptible to thermal gradients<sup>54,55</sup>.

Figure 4b shows fine particulate (<125  $\mu\text{m}$ ) versions of the same meteorite samples measured by K.L.D.H. in a simulated asteroid environment at Oxford University; the sample preparation, characterization, and spectral measurements are described in detail by<sup>56</sup>. The <90- $\mu\text{m}$  magnetite spectrum in Figure 5 was measured under the same conditions and its spectrum is virtually identical to magnetite spectra measured as coarse materials and under ambient conditions. All of these spectra are appropriate for comparison to OTES emissivity spectra of dominantly fine particulates that exhibit volume scattering and are potentially susceptible to the development of thermal gradients.

### Data Availability Statement

The data that support the plots within this paper and other findings of this study are available from the corresponding author upon reasonable request. Raw and calibrated spectral data will be available via the Small Bodies Node of the Planetary Data System (PDS) (<https://pds-smallbodies.astro.umd.edu/>). Data are delivered to the PDS according to the OSIRIS-REx Data Management Plan available in the OSIRIS-REx PDS archive. Higher-level products, such as reflectance and emissivity spectra, will be available in the PDS 1 (one) year after departure from the asteroid. Laboratory spectral data are deposited in the spectral library hosted by Arizona State University (<http://speclib.mars.asu.edu/>).

### Acknowledgements

This material is based upon work supported by NASA under Contract NNM10AA11C issued through the New Frontiers Program. T. Burbine, F. S. Anderson, and J. Joseph provided considerable assistance with early software development for the spectral analysis working group. H. Campins, R. Binzel, and E. Dotto participated in discussions of space weathering and the spectral results. C. Wolner provided helpful copyediting support. The J-Asteroid software tool and development team at ASU enabled visualization of the spectral data that was critical to the analysis. The authors also extend their gratitude to the following people without whom this work would not have been possible: the instrument teams at NASA Goddard Spaceflight Center (GSFC) and Arizona State University; the spacecraft teams at GSFC, KinetX, and Lockheed Martin; the science planning and operations teams at the University of Arizona; and the Science Processing and Operations Center staff at the University of Arizona.

INAF is supported by Italian Space Agency agreement n. 2017–37-H.0. The French co-authors acknowledge support from CNES. BR acknowledges the support of the Royal Astronomical Society in the form of a research fellowship.

## References

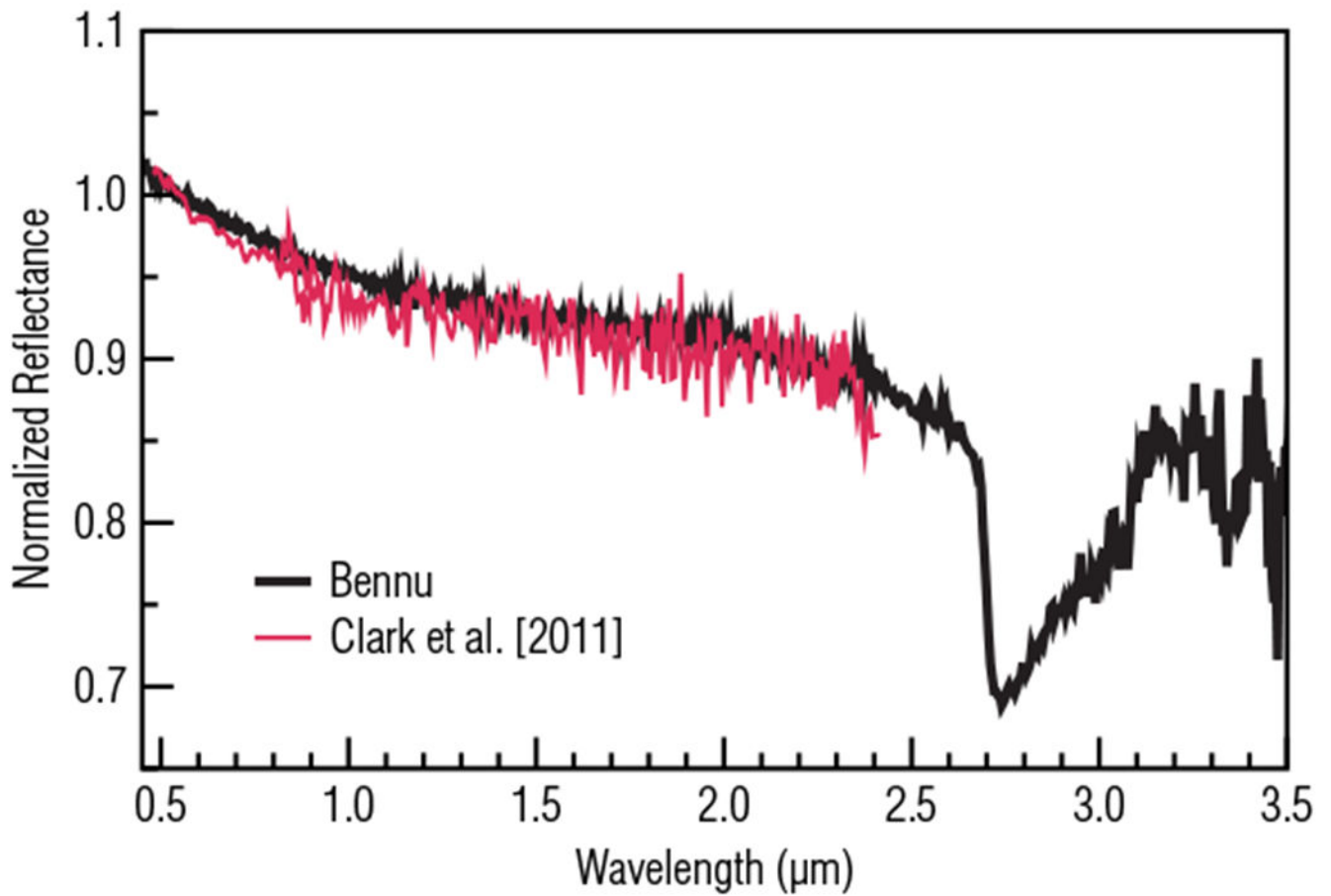
1. Clark BE et al. Asteroid (101955) 1999 RQ36: Spectroscopy from 0.4 to 2.4  $\mu\text{m}$  and meteorite analogs. *Icarus* 216, 462–475 (2011).
2. Reuter DC et al. The OSIRIS-REx Visible and InfraRed Spectrometer (OVIRS): Spectral Maps of the Asteroid Bennu. *Space Sci. Rev* 214, doi: 10.1007/s11214-018-0482-9 (2018).
3. Christensen PR et al. The OSIRIS-REx Thermal Emission Spectrometer (OTES) instrument. *Space Sci. Rev* 214, doi:0.1007/s11214-018-0513-6 (2018).
4. Lauretta DS et al. OSIRIS-REx: Sample return from asteroid (101955) Bennu. *Space Sci. Rev* 212, 925–984, doi: 10.1007/s11214-017-0405-1 (2017).
5. DellaGiustina DN, Emery JP, et al., Surface properties of Bennu from imaging and thermal observations. Submitted to *Nat. Astron* (this package).
6. Rizk B et al. OCAMS: The OSIRIS-REx camera suite. *Space Sci. Rev* 214, 26 (2018).
7. Van Schmus WR & Wood JA A chemical-petrologic classification for the chondritic meteorites. *Geochim. Cosmochim. Acta* 31, 747–765 (1967).
8. Binzel RP et al. Spectral slope variations for OSIRIS-REx target asteroid (101955) Bennu: Possible evidence for a fine-grained regolith equatorial ridge. *Icarus* 256, 22–29 (2015).
9. Cloutis EA, Hiroi T, Gaffey MJ & Alexander CMOD Spectral reflectance properties of carbonaceous chondrites: 1. CI chondrites. *Icarus* 212, 180–209 (2011).
10. Cloutis EA, Hudon P, Hiroi T, Gaffey MJ & Mann P Spectral reflectance properties of carbonaceous chondrites: 2. CM chondrites. *Icarus* 216, 309–346 (2011).
11. Thompson MS, Loeffler MJ, Morris RV, Keller LP & Christofferson R Spectral and chemical effect of simulated space weathering of the Murchison CM2 carbonaceous chondrite. *Icarus* 319, 499–511 (2019).
12. Lauretta DS, DellaGiustina DN, et al. The unexpected surface of asteroid (101955) Bennu and challenges for the OSIRIS-REx sample return mission. Submitted to *Nature* (this package).
13. Izawa MRM et al. Spectral reflectance properties of magnetites: Implications for remote sensing. *Icarus* 319, 525–539 (2019).
14. Brunetto R et al. Ion irradiation of Allende meteorite probed by visible, IR, and Raman spectroscopies. *Icarus* 237, 278–292 (2014).
15. Lantz C, Binzel RP & DeMeo FE Space weathering trends on carbonaceous asteroids: A possible explanation for Bennu’s blue slope? *Icarus* 302, 10–17 (2018).
16. Miyamoto M & Zolensky ME Infrared diffuse reflectance spectra of carbonaceous chondrites: Amount of hydrous materials. *Meteoritics* 29, 849–853 (1994).
17. Moroz LV, Schmidt M, Schade U, Hiroi T & Ivanova MA Synchrotron-based infrared microspectroscopy as a useful tool to study hydration states of meteorite constituents. *Meteorit. Planet. Sci* 41, 1219–1230 (2006).
18. Beck P et al. Hydrous mineralogy of CM and CI chondrites from infrared spectroscopy and their relationship with low albedo asteroids. *Geochim. Cosmochim. Acta* 74, 4881–4892 (2010).
19. Takir D et al. Nature and degree of aqueous alteration in CM and CI carbonaceous chondrites. *Meteorit. Planet. Sci* 48, 1618–1637 (2013).
20. Zolensky ME & McSween HY Jr. in *Meteorites and the Early Solar System* (eds Kerridge JF & Matthews MS) pp. 114–143 (University of Arizona Press, Tucson, AZ, 1988).
21. Brearley AJ & Jones RH in *Rev. Mineral Vol. 36 Ch. 3*, 3.1–3.398 (1998).
22. Abreu NM Fine-scale mineralogical study of the matrices of CR carbonaceous chondrites: Insights on early solar system processes Ph.D. thesis, The University of New Mexico, (2007).
23. Bishop JL, Lane MD, Dyar MD & Brown AJ Reflectance and emission spectroscopy study of four groups of phyllosilicates: smectites, kaolinite-serpentines, chlorites and micas. *Clay Minerals* 43, 35–54 (2008).

24. Lantz C et al. Ion irradiation of the Murchison meteorite: Visible to mid-infrared spectroscopic results. *Astron. Astrophys* 577, A41, doi: 10.1051/0004-6361/201425398 (2015).
25. Rivkin AS et al. in *Asteroids IV* (ed Michel P, et al.) 65–87 (University of Arizona, 2015).
26. Takir D & Emery JP Outer main belt asteroids: Identification and distribuion of four 3- $\mu$ m spectral groups. *Icarus* 219, 641–654 (2012).
27. Rivkin AS, Howell ES, Emery JP, Volquardsen EL & DeMeo FE Toward a taxonomy of asteroid spectra in the 3- $\mu$ m region. *European Planet. Sci. Congr* 7, 359 (2012).
28. Rivkin AS & Emery JP Detection of ice and organics on an asteroidal surface. *Nature* 464, 1322–1323 (2010). [PubMed: 20428165]
29. Campins H et al. Water ice and organics on the surface of the asteroid 24 Themis. *Nature* 464, 1320–1321, doi:10.1038/nature09029 (2010). [PubMed: 20428164]
30. Sugita S et al. The geomorphology, color, and thermal properties of Ryugu: Implications for parent-body processes. *Science* (submitted).
31. Kitazato K et al. Surface composition of asteroid 162173 Ryugu as observed by the Hayabusa2 NIRS3 instrument. *Science* (submitted).
32. Emery JP et al. Thermal infrared observations and thermophysical characterization of OSIRIS-REx target asteroid (101955) Bennu. *Icarus* 234, 17–35, doi:10.1016/j.icarus.2014.02.005 (2014).
33. Lim LF. The global thermal infrared spectrum of Bennu: Comparison with Spitzer IRS asteroid spectra; Abstract P33C-3844 presented at 2018 AGU Fall Meeting; Washington, D.C.. Dec, 2018 3810–3814.
34. Howard KT, Alexander CMOD, Schrader DL & Dyl KA Classification of hydrous meteorites (CR, CM and C2 ungrouped) by phyllosilicate fraction: PSD-XRD modal mineralogy and planetesimal environments. *Geochim. Cosmochim. Acta* 149, 206–222 (2015).
35. King AJ, Schofield PF & Russell SS Type 1 aqueous alteration in CM carbonaceous chondrites: Implications for the evolution of water-rich asteroids. *Meteorit. Planet. Sci* 52, 1197–1215 (2017).
36. McSween HY Jr. Are carbonaceous chondrites primitive or processed? A review. *Rev. Geophys. Space Phys* 17, 1059–1078(1979).
37. Morlok A et al. Brecciation and chemical heterogeneity of CI chondrites. *Geochim. Cosmochim. Acta* 70, 5371–5394 (2006).
38. Rubin AE, Trigo-Rodriguez JM, Huber H & Wasson JT Progressive aqueous alteration of CM carbonaceous chondrites. *Geochim. Cosmochim. Acta* 71, 2361–2382 (2007).
39. Hamilton VE et al. Spectral classification of ungrouped carbonaceous chondrites II: Parameters and comparison to independent measures. *Lunar and Planetary Science XLIX*, Abstract #1753 (2018).
40. Hamilton VE Thermal infrared emission spectroscopy of the pyroxene mineral series. *J. Geophys. Res* 105, 9701–9716 (2000).
41. Hamilton VE Thermal infrared (vibrational) spectroscopy of Mg-Fe olivines: A review and applications to determining the composition of planetary surfaces. *Chem. Erde* 70, 7–33, doi: 10.1016/j.chemer.2009.12.005 (2010).
42. Walsh KJ et al. The mature and dynamic surface geology of Bennu. Submitted to *Nat. Geosci* (this package).
43. Scheeres DJ et al. The global geophysical environment of (101955) Bennu. Submitted to *Nat. Astron* (this package).

### Additional references only in the Methods

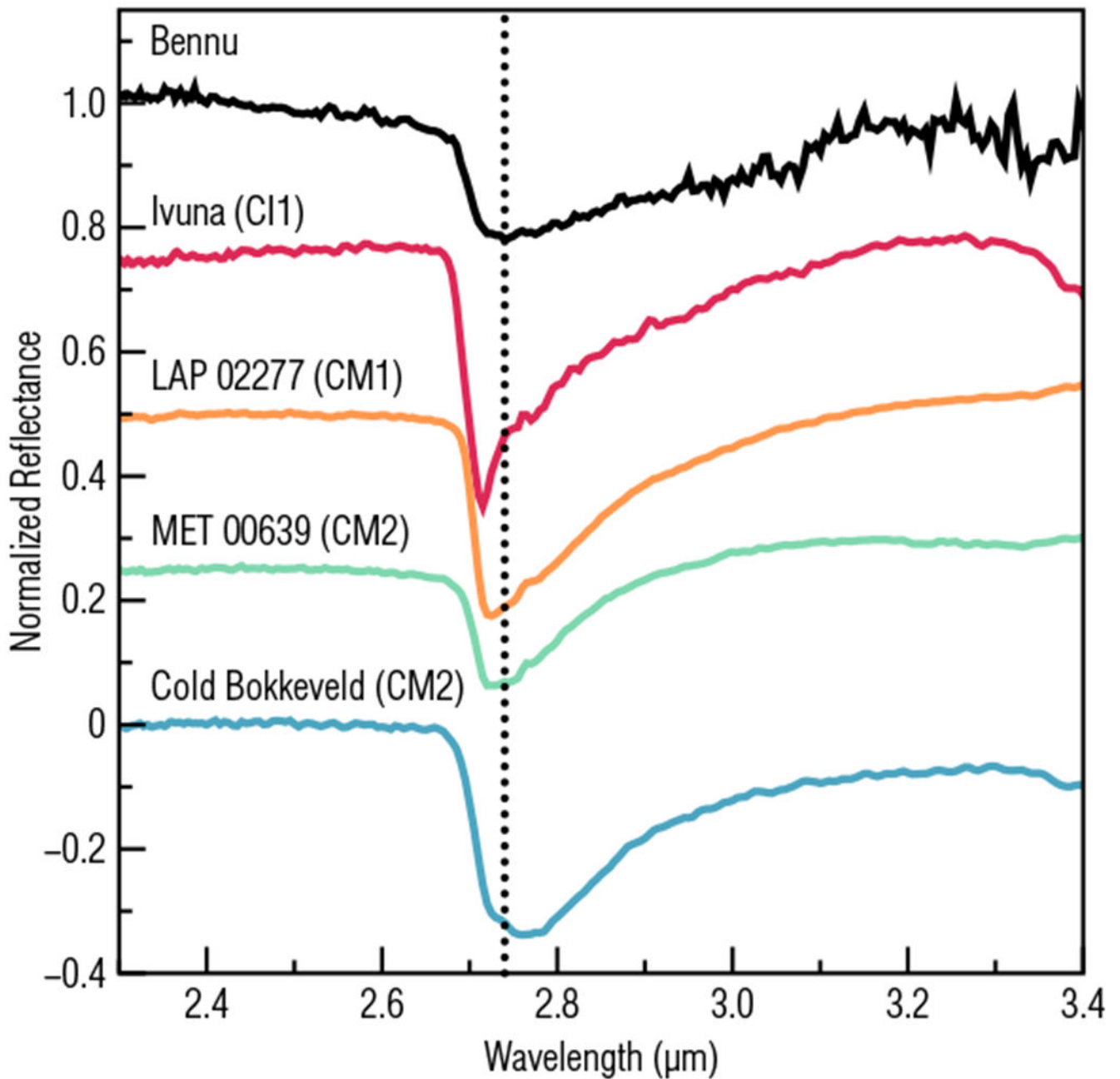
44. Reuter DC et al. Ralph, A visible/infrared imager for the New Horizons Pluto/Kuiper Belt mission. *Space Sci. Rev* 140, 129–154 (2008).
45. Simon AA et al. In-flight calibration and performance of the OSIRIS-REx Visible and IR Spectrometer (OVIRS). *Remote Sensing* 10, 1486 (2018).
46. Hergenrother CW et al. Photometric properties, rotational acceleration, and operational environment of asteroid (101955) Bennu from OSIRIS-REx observations. *Nat. Comms* (this package).

47. Barnouin OS et al. Exploring the shape of (101955) Bennu with OSIRIS-REx. Submitted to Nat. Geosci (this package).
48. Christensen PR et al. Mars Global Surveyor Thermal Emission Spectrometer experiment: Investigation description and surface science results. *J. Geophys. Res* 106, 23,823–823,871 (2001).
49. Christensen PR et al. Miniature Thermal Emission Spectrometer for the Mars Exploration Rovers. *J. Geophys. Res* 108, 8064, doi:10.1029/2003JE002117 (2003).
50. Rogers AD & Aharonson O. Mineralogical composition of sands in Meridiani Planum determined from Mars Exploration Rover data and comparison to orbital measurements. *J. Geophys. Res* 113, E06S14, doi:10.1029/2007JE002995 (2008).
51. Quirico E et al. Origin of insoluble organic matter in type 1 and 2 chondrites: New clues, new questions. *Geochim. Cosmochim. Acta* 136, 80–99 (2014).
52. Quirico E et al. Prevalence and nature of heating processes in CM and C2-ungrouped chondrites as revealed by insoluble organic matter. *Geochim. Cosmochim. Acta* 241, 17–37 (2018).
53. Hamilton VE Spectral classification of ungrouped carbonaceous chondrites I: Data collection and processing. *Lunar and Planetary Science XLIX*, Abstract #1759 (2018).
54. Logan LM & Hunt GR Emission spectra of particulate silicates under simulated lunar conditions. *J. Geophys. Res* 75, 6539–6548 (1970).
55. Henderson BG & Jakosky BM Near-surface thermal gradients and mid-IR emission spectra: A new model including scattering and application to real data. *J. Geophys. Res* 102, 6567–6580 (1997).
56. Donaldson Hanna KL et al. Spectral characterization of analog samples in anticipation of OSIRIS-REx's arrival at Bennu: A blind test study. *Icarus* 319, 701–723, doi: 10.1016/j.icarus.2018.10.018 (2019).



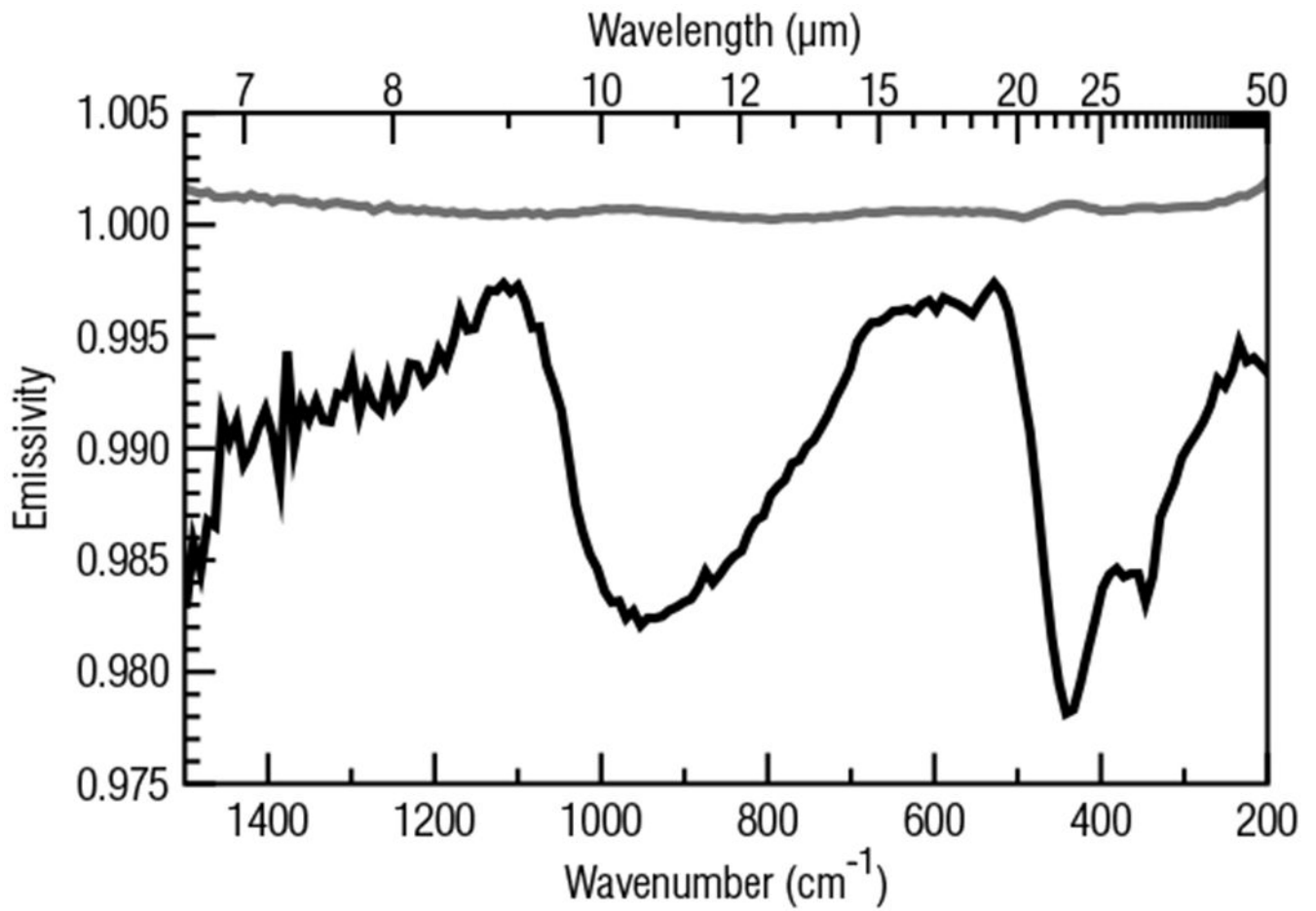
**Figure 1. Average whole-disk, full-rotation OVIRS spectrum of Bennu compared with the ground-based spectrum.**

The OVIRS radiance factor spectrum (black) and ground-based spectrum<sup>1</sup> (red) are normalized to a reflectance of 1.0 at 0.55  $\mu\text{m}$ . The OVIRS data were acquired on day of year (DOY) 306 (2 November 2018), and the field of view was  $\sim 40\%$  filled during these observations.

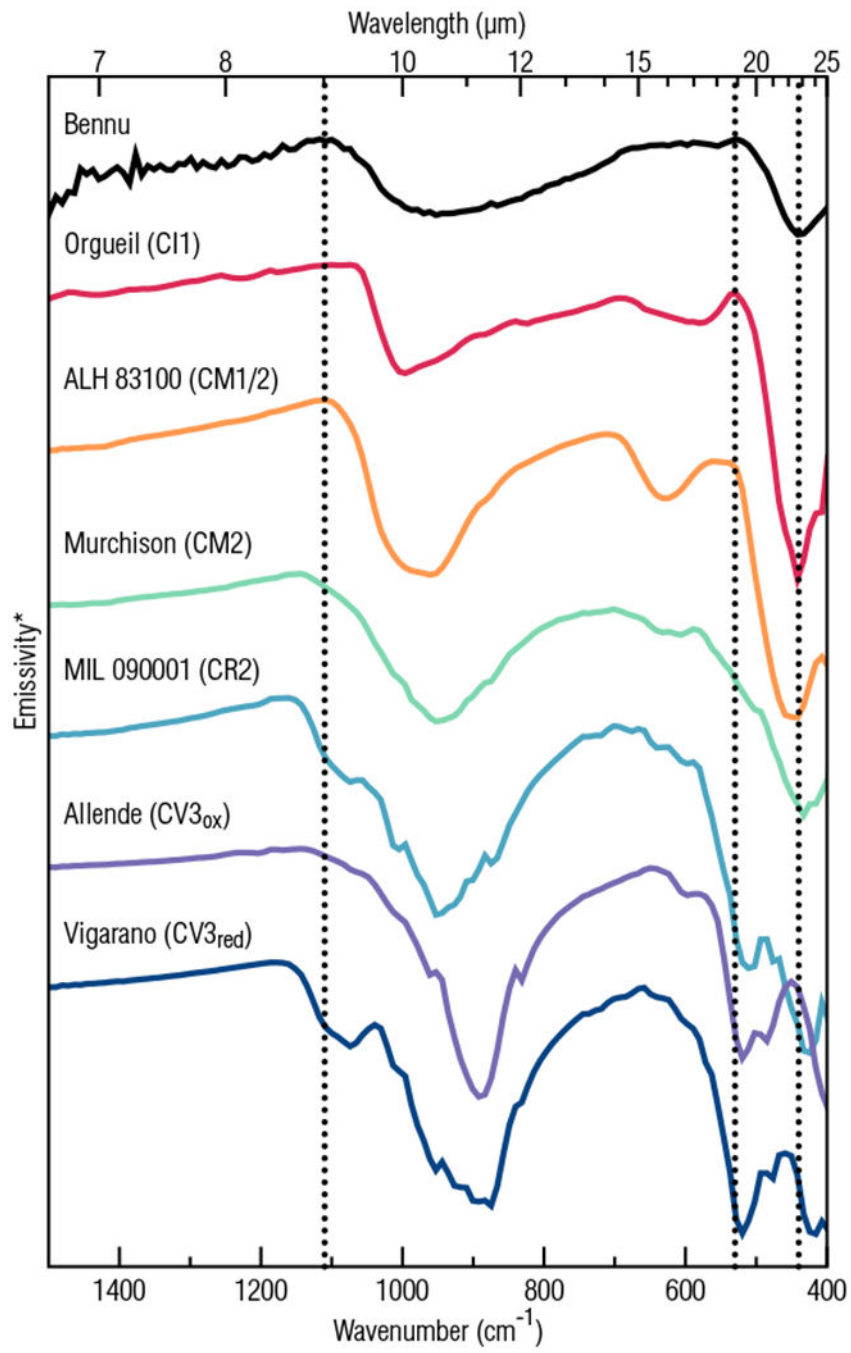


**Figure 2. Average DOY 306 OVIRS spectrum between 2.3 and 3.5  $\mu\text{m}$  compared to spectra of example carbonaceous chondrites.**

The carbonaceous chondrites were measured in vacuum after heating<sup>19</sup> (see Methods for full meteorite names). The spectra are normalized to a reflectance of 1.0 at 2.4  $\mu\text{m}$  and offset vertically for clarity. The vertical line at 2.74  $\mu\text{m}$  denotes the Benu band minimum position (see Methods).



**Figure 3.** Average OTES spectrum of Benu between 1500 and 200  $\text{cm}^{-1}$ . The Benu spectrum (black) represents slightly more than one full rotation of the asteroid as measured on DOY 347 (13 December 2018). The gray spectrum shows the standard deviation (offset +0.98).



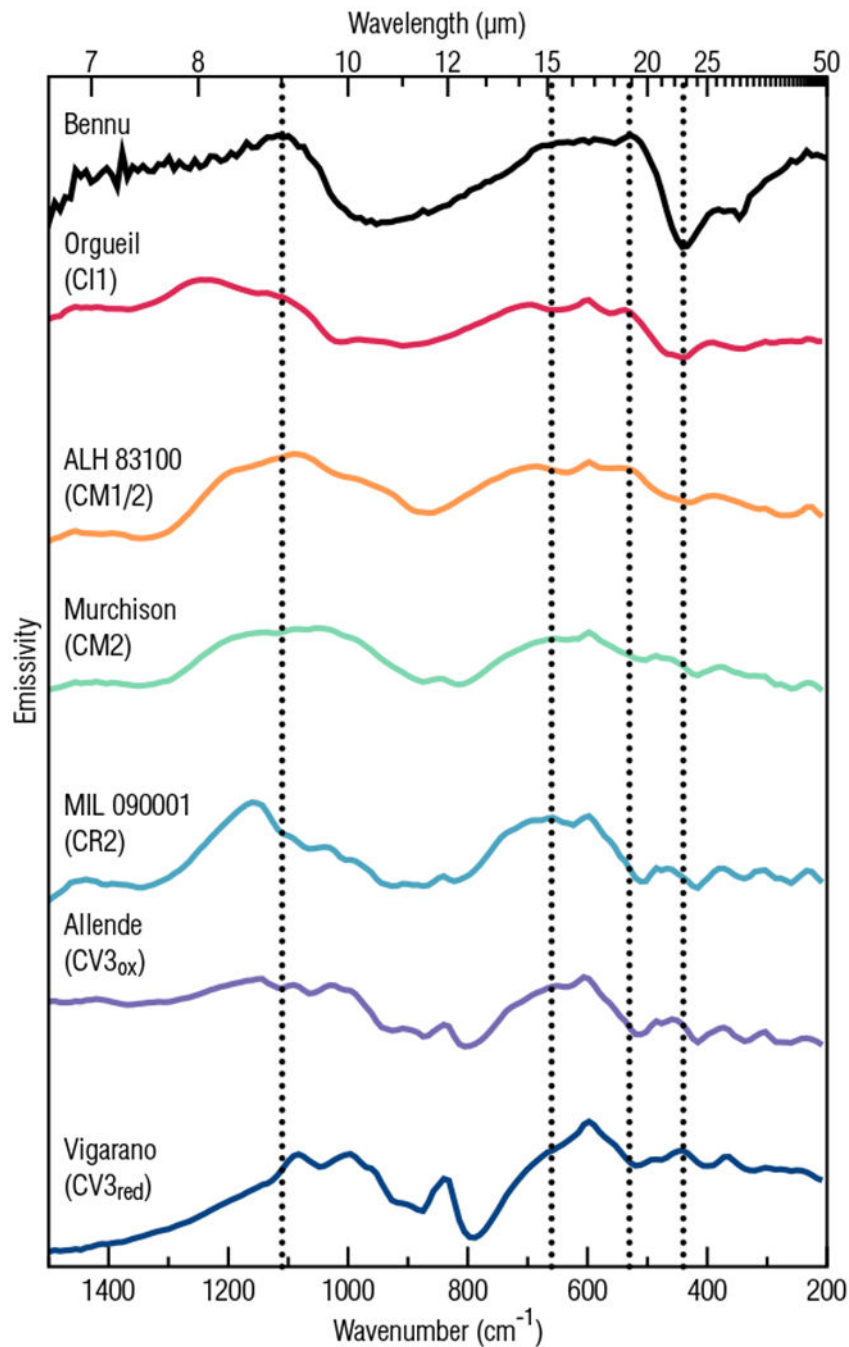


**Figure 4. Average OTES spectrum of Benu compared to spectra of whole-rock and fine-particulate carbonaceous chondrite meteorites.**

**a.** Comparison with whole-rock samples, **b.** Comparison with fine-particulate (<125  $\mu\text{m}$ ) samples. Spectra have been scaled and offset for comparison (see Methods). Vertical lines at 1110 and 530  $\text{cm}^{-1}$  indicate the positions of diagnostic peaks in the Benu spectrum, and the vertical line at 440  $\text{cm}^{-1}$  denotes a diagnostic absorption.

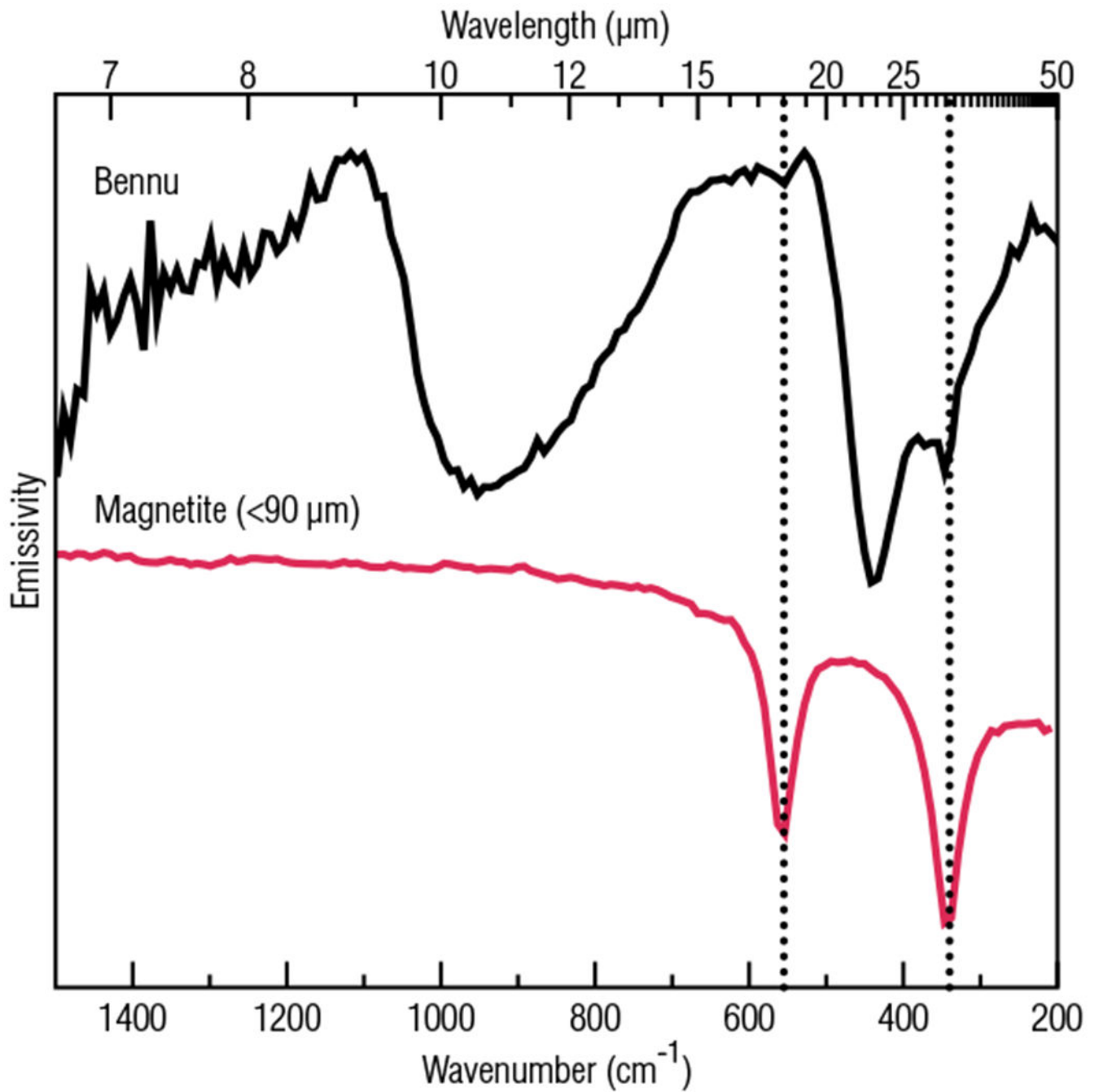


**Figure 5. Average OTES Bennu spectrum compared to a spectrum of pure, fine-particulate (<90 μm) magnetite.**

Spectra have been scaled and offset for comparison. Vertical lines at 555 and 340 cm<sup>-1</sup> indicate the positions of diagnostic absorptions in both spectra.